4852 *Biochemistry* **2009,** *48,* 4852–4857
DOI: 10.1021/bi900014d

BIOCHEMISTRY
including biophysical chemistry & molecular biology
Article

A22 Disrupts the Bacterial Actin Cytoskeleton by Directly Binding and Inducing a Low-Affinity State in MreB[†]

G. J. Bean,[‡] S. T. Flickinger,[§] W. M. Westler,[∥] M. E. McCully,[⊥] D. Sept,[⊥] D. B. Weibel,[§,@] and K. J. Amann*[,‡,#]

[‡]*Laboratory of Molecular Biology, University of Wisconsin, 1525 Linden Drive, Madison, Wisconsin 53706,* [§]*Department of Biochemistry, University of Wisconsin, 433 Babcock Drive, Madison, Wisconsin 53706,* [∥]*National Magnetic Resonance Facility at Madison, 433 Babcock Drive, Madison, Wisconsin 53706,* [⊥]*Department of Biomedical Engineering and Center for Computational Biology, Washington University, St. Louis, Missouri 63130,* [@]*Department of Biomedical Engineering, University of Wisconsin, 1550 Engineering Drive, Madison, Wisconsin 53706, and* [#]*Department of Zoology, University of Wisconsin, 1525 Linden Drive, Madison, Wisconsin 53706*

Received January 6, 2009; Revised Manuscript Received April 3, 2009

ABSTRACT: *S*-(3,4-Dichlorobenzyl)isothiourea (A22) disrupts the actin cytoskeleton of bacteria, causing defects of morphology and chromosome segregation. Previous studies have suggested that the actin homologue MreB itself is the target of A22, but there has been no direct observation of A22 binding to MreB and no mechanistic explanation of its mode of action. We show that A22 binds MreB with at least micromolar affinity in its nucleotide-binding pocket in a manner that is sterically incompatible with simultaneous ATP binding. A22 negatively affects both the time course and extent of MreB polymerization in vitro in the presence of ATP. A22 prevents assembly of MreB into long, rigid polymers, as determined by both fluorescence microscopy and sedimentation assays. A22 increases the critical concentration of ATP-bound MreB assembly from 500 nM to approximately 2000 nM. We therefore conclude that A22 is a competitive inhibitor of ATP binding to MreB. A22-bound MreB is capable of polymerization, but with assembly properties that more closely resemble those of the ADP-bound state. Because the cellular concentration of MreB is in the low micromolar range, this mechanism explains the ability of A22 to largely disassemble the actin cytoskeleton in bacterial cells. It also represents a novel mode of action for a cytoskeletal drug and the first biochemical characterization of the interaction between a small molecule inhibitor of the bacterial cytoskeleton and its target.

Despite prior assumptions to the contrary, bacteria have cytoskeletons comprised of tubulin (*1*, *2*), actin (*3*, *4*), and intermediate filament (*5*) homologues. While the cellular functions of these molecules differ significantly from their canonical behaviors in eukaryotic cells, they are increasingly understood to control the morphology and division of a wide variety of bacteria (*6*). The bacterial actin, MreB, is required for establishment and maintenance of the characteristic rod shape (*7*), cell division (*3*, *8*), chromosome segregation (*9*−*11*), cell wall morphogenesis (*12*), and cell polarity (*13*) and even plays a role in the localization of the chromosome replication machinery (*14*) in species ranging from Gram-negative (*Escherichia coli*) to Gram-positive (*Bacillus subtilis* and *Caulobacter crescentus*) bacteria.

S-(3,4-Dichlorobenzyl)isothiourea (A22)[1] was identified by virtue of its ability to induce spherical anucleate cells in the rod-shaped bacterium *E. coli* (*15*). The treatment of cells with A22 disrupts the helical localization of MreB in vivo and appears to cause its disassembly, which leads to the diffuse distribution of MreB in the cytoplasm and loss of rod-shaped cell morphology and viability (*16*, *17*). Despite the widespread use of A22 to disrupt MreB and bacterial morphology (*16*−*28*), to date there has been no experimental evidence of a direct interaction between A22 and MreB and no mechanistic study of the mode of action of A22.

We sought to test and characterize the interaction between A22 and MreB and to discern its mechanism of action. We found that A22 is a competitive inhibitor of ATP binding by MreB and that its binding induces a state in MreB capable of polymerizing, but

[†]This work was supported by American Heart Association Scientist Development Grant 0430162N and National Science Foundation (NSF) Grant 0818946 to K.J.A.; awards by the Searle Scholar Program and 3M Corp. and a Human Frontiers Science Program grant to D.B. W.; and National Institutes of Health (NIH) Grant GM067246 to D.S. This study made use of the National Magnetic Resonance Facility at Madison, which is supported by NIH Grants P41RR02301 (BRTP/NCRR) and P41GM66326 (NIGMS). Additional equipment was purchased with funds from the University of Wisconsin, the NIH (RR02781 and RR08438), the NSF (DMB-8415048, OIA-9977486, and BIR-9214394), and the U.S. Department of Agriculture.

*To whom correspondence should be addressed: Laboratory of Molecular Biology and Department of Zoology, University of Wisconsin, 335A R. M. Bock Laboratories, 1525 Linden Dr., Madison, WI 53706. Telephone: (608) 265-3150. Fax: (608) 262-4570. E-mail: kjamann@wisc.edu.

[1]Abbreviations: GTP, guanosine triphosphate; SDS−PAGE, sodium dodecyl sulfate−polyacrylamide gel electrophoresis; EGTA, ethylene glycol tetraacetic acid; A22, *S*-(3,4-dichlorobenzyl)isothiourea.

Published on Web 04/21/2009

at a greatly reduced affinity for polymerization. These results explain the disassembly of MreB polymers by A22 in cells. They also represent a novel mode of action for any cytoskeletal drug and the first biochemical characterization of the interaction of any drug with the bacterial cytoskeleton.

EXPERIMENTAL PROCEDURES

Proteins. Untagged *Thermotoga maritima* MreB1 was overexpressed and purified from *E. coli* as previously described (*29*) and stored in CaG8 buffer without DTT [2 mM Tris-HCl (pH 8.0), 0.1 mM $CaCl_2$, 200 μM ATP, and 0.02% NaN_3]. ADP-MreB was prepared by Dowex treatment as previously described (*ref29*). Cys332-substituted MreB and Alexa488-labeled MreB were produced as previously described (*29*). *T. maritima* MreB1-his was constructed as follows: *mreB1* was amplified from genomic DNA using forward and reverse primers 5′GGGAATTCCATATGTTGAGAAAAGACATAGGAATAGATC3′ and 5′ATAAGAATGTCGACCCCGGCACCCTGAAGCTTCTTC3′, respectively, digested with NdeI and SalI, and ligated into the NdeI and XhoI site of pET23a. MreB1-his was expressed in BL21(DE3)pLysS cells, extracted in NiG8 buffer, purified by Ni-agarose chromatography, eluted with imidazole in CaG8 buffer, dialyzed against 10 mM Tris-HCl (pH 8.0) without nucleotide, and stored at −80 °C until use. All proteins were quantified by SDS−PAGE/Coomassie Blue densitometry in ImageJ using rabbit actin as a standard. With the exception of NMR, all experiments herein were performed using untagged MreB1.

MreB Polymerization. Unless stated otherwise, non-protein reaction components were mixed on ice in proportions such that the final reaction mixtures contained 200 μM ATP, 10 mM imidazole (pH 7.0), 20 mM KCl, 1 mM $MgCl_2$, and 1 mM EGTA (KMEI). Separately on ice, MreB in CaG8 storage buffer was mixed with $^1/_9$ volume of 10× cation exchange buffer (1 mM $MgCl_2$ and 10 mM EGTA) and incubated on ice for 1 min. Polymerization was initiated by combining the two samples with gentle mixing.

Light Scattering. The 90° perpendicular light scattering experiments were conducted as previously described (*29*) using a PC1 spectrofluorometer (ISS) equipped with a temperature control jacket and under control of Vinci software (ISS) version 1.4.9.5. Excitation and emission monochrometers were set at 400 nm, and slit pairs (typically 1 mm) were employed in both excitation and emission paths. Data were collected at 1 s intervals, analyzed in Excel, and plotted using Kaleidagraph.

Critical Concentration. MreB was polymerized as described above at varying protein concentrations. Reaction mixtures were equilibrated for 1 h at the experimental temperature prior to measurement of light scattering intensity as described above. Light scattering values were the average of 1 min of acquired signal. Critical concentrations were determined by the intersection of two linear fits to the data points above and below the apparent inflection point in the graph as determined by visual inspection.

Sedimentation. MreB was polymerized as described and centrifuged either at 4 °C for 30 min at 100000*g* in a Beckman tabletop ultracentrifuge or at room temperature for 10 min at 100000*g* in a Beckman airfuge. Supernatant and pellet fractions were separated and analyzed by SDS−PAGE, stained with Coomassie Blue, and quantitated by densitometry.

Fluorescence Microscopy. Alexa488-labeled L332C MreB and unlabeled native MreB were mixed and polymerized at room temperature for 1 h in standard buffer conditions at a total concentration of 1 μM. Samples were applied directly to coverslips and viewed on an Olympus IX-71 epifluorescence microscope using a 60× 1.45 n.a. objective lens and fluorescein filter set (Chroma). Images were acquired using a Hamamatsu Orca 285 camera under control of Wasabi software. Image manipulation, limited to global contrast and brightness enhancement, was conducted in Adobe Photoshop CS2. Polymer lengths were measured manually and analyzed using Excel and Kaleidagraph.

A22. A22 was synthesized from 3,4-dichlorobenzyl chloride and thiourea and purified by recrystallization from diethyl ether three times. Spectral data for the compound matched those reported previously (*15*).

STD NMR. NMR experiments were performed at 10 °C on a 750 MHz Bruker DMX spectrometer equipped with a 5 mm triple-resonance cryogenic probe. A saturation transfer difference pulse sequence with a saturation frequency at −1 ppm and an off-resonance saturation frequency at −40 ppm was used with a standard one-dimensional proton spectrum as described in the literature (*30*). NMR samples consisted of 600 μL of a solution of his-tagged MreB in Tris buffer (10 mM, pH 8.0), 70 μL of D_2O, and 30 μL of a solution of A22 in DMSO-d_6; the total sample volume was 700 μL. The final concentration of A22 in each NMR sample was 5 mM; the concentration of MreB in the samples varied from 0 to 12.8 μM. Deuterium oxide (D_2O) was purchased from Cambridge Isotope Laboratories, Inc. (Andover, MA), and (methyl sulfoxide)-d_6 (DMSO-d_6) was from Sigma-Aldrich (St. Louis, MO).

We processed NMR data using NutsPro (Acorn NMR). The free induction decay was filtered with a 90° phase-shifted, sine-squared function, and the resulting data were zero-filled and transformed using a Fourier function. A baseline correction was performed on the transformed spectra. We used line fitting scripts to determine the area of the peaks that corresponded to the three aromatic protons of A22. We fit data using Prism 4.0 (GraphPad Software) to a one-site binding model of the form

$$Y = \frac{B_{max} X}{K_d + X}$$

where Y is the integrated area under the NMR peak, X is the concentration of MreB (micromolar), K_d is the dissociation constant, and B_{max} is the theoretical maximum intensity at saturation binding. The individual data sets were normalized between their integrated peak areas at zero protein concentration and their fitted B_{max} values, resulting in a response range from 0 to 1.0. To determine the lower limit of the K_d of A22 bound to MreB, the data sets were combined and fit to the one-site binding model described above.

Docking. The starting point for the docking studies was the crystal structure of MreB bound with AMPPNP (Protein Data Bank entry 1JCG) (*4*) where we modified the AMP-PNP to make ATP. For A22, we constructed the compound in Sybyl 6.8 (Tripos Inc., St. Louis, MO) and assigned Gasteiger-Marsili charges to MreB, ATP, and A22. We performed two sets of docking studies: one to place A22 on the MreB−ATP complex and one to dock A22 to the nucleotide-free form of MreB. Both docking runs were carried out using AutoDock 3.0 (*31*) with 0.375 Å spacing and 50 independent runs using the Lamarckian genetic algorithm with 10 million energy evaluations. The docking results were clustered using a 1.0 Å root-mean-square deviation and analyzed for both their predicted docking energy

and cluster size. Additional docking studies were conducted using MreB mutants T158A and V315A as well as 2,3-dichlorobenzyl and 2,4,6-trichlorobenzyl derivatives of A22.

RESULTS

A22 Binds MreB with Micromolar Affinity. We used saturation transfer difference (STD) NMR to test for a direct interaction between A22 and MreB-his in the absence of free ATP. Because MreB is not monomeric at very high concentrations, even in low-salt storage buffer, we used a high concentration of A22 (5 mM) and varied the concentration of MreB over a range from 0 to 12.8 μM. We chose the three aromatic protons of A22 for our STD analysis because they were well resolved from the other peaks in the NMR spectra (e.g., buffer, solvents). We collected and normalized NMR data sets, plotted the peak areas of the three aromatic protons versus MreB concentration, and fit it to a one-site binding model to estimate the K_d (Figure 1). The curve fit yielded a K_d of 1.32 $\pm$ 0.14 μM (R^2 = 0.89) for A22 binding to MreB. Because this experiment measures a saturation transfer difference, the observed peak areas are amplified by a factor equal to k_{off} (i.e., observed peak area = k_{off}[PL]). An apparent larger value of the protein−ligand complex would result in an apparent smaller K_d (since K_d = [P][L]/[PL]). Therefore, the estimated K_d that we report represents a lower limit for the affinity.

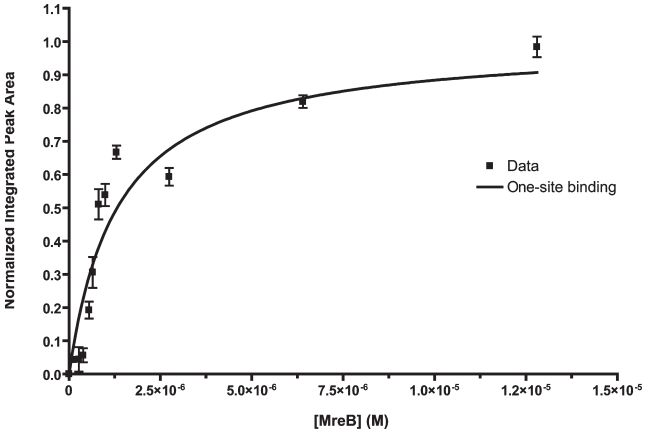

FIGURE 1: A22−MreB interaction observed by NMR. A22 (5 mM) was incubated with varying concentrations of MreB in 10 mM Tris-HCl (pH 8.0) at 10 °C. Normalized integrated peak areas collected for the three aromatic protons in A22 were plotted vs protein concentration and fitted to a one-site binding model. The K_d was found to be 1.32 $\pm$ 0.14 μM (R^2 = 0.89).

The A22 Binding Site Overlaps with the Nucleotide. To determine where A22 binds on the MreB structure, we performed a series of small molecule docking studies. When we used the ATP-bound form of MreB, A22 docked in a nonspecific, nonreproducible manner over the surface of MreB with indeterminate binding affinity. When we removed the nucleotide and repeated the docking studies, A22 bound with high affinity (~0.19 μM) and specificity in the nucleotide-binding site (see Figure 2). A22 interacts primarily with E131 and T158 of MreB, both highly conserved (see Discussion). The aromatic ring and thiourea group of A22 overlap with the positions that would be occupied by the nucleotide's β- and γ-phosphates, respectively. Together, these results suggest that A22 functions as a competitive inhibitor of ATP. Docking studies using T158A or V315A MreB mutants binding to A22 or MreB binding to 2,3-dichlorobenzyl or 2,4,6-trichlorobenzyl derivatives of A22 yielded uniformly weaker binding (not shown).

Fluorescence Microscopy: A22 Prevents MreB Polymer Assembly. We investigated the effects of A22 on the assembly and morphology of MreB polymers by fluorescence microscopy. We made use of C332-substituted MreB covalently labeled with Alexa488 to visualize polymers by epifluorescence microscopy. When 1 μM MreB was incubated under standard polymerizing conditions for 1 h and applied directly to glass sides, the product of the reaction was long, rigid polymers (Figure 3A) as previously observed (*29*). When identical reactions were conducted in the presence of 300 μM A22, however, no linear structures were observed; instead, only small ($<$1 μm), amorphous fluorescent structures were seen.

Light Scattering Time Course: A22 Affects the Time Course of MreB Assembly. We further studied the effects of A22 on MreB by following the time course of polymerization by light scattering (Figure 4). In the absence of A22, and under standard polymerization conditions, 5 μM ATP-bound MreB assembly followed a time course that clearly exhibited the lag (nucleation), linear (polymerization), and plateau (steady-state) phases of actin assembly. When A22 was included at increasing concentrations, the rate and extent of MreB assembly were reduced. Maximal inhibition was observed at an A22 concentration of 300 μM. At higher A22 concentrations, nonspecific,

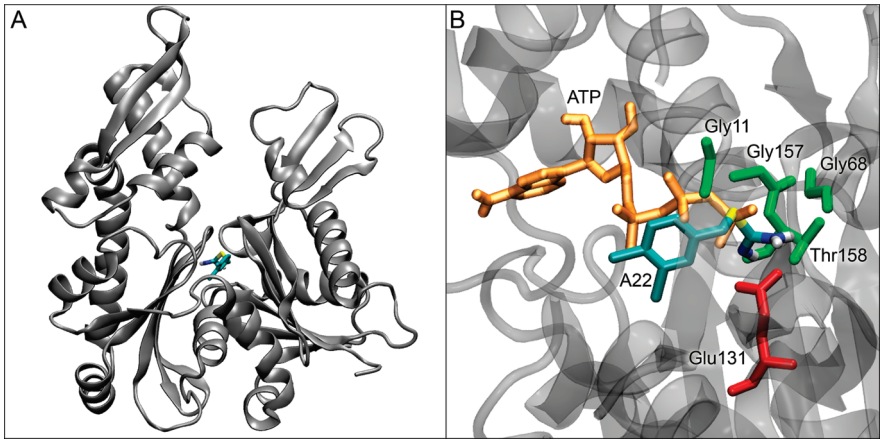

FIGURE 2: A22 docking in the MreB nucleotide cleft. (A) Docking site of A22 in the nucleotide-free form of MreB. (B) Details of the binding site of A22 in MreB with residues within 2.5 Å of A22 shown with their side chains. ATP is shown in its crystal position, illustrating the clashes that would occur between its β- and γ-phosphates and A22.

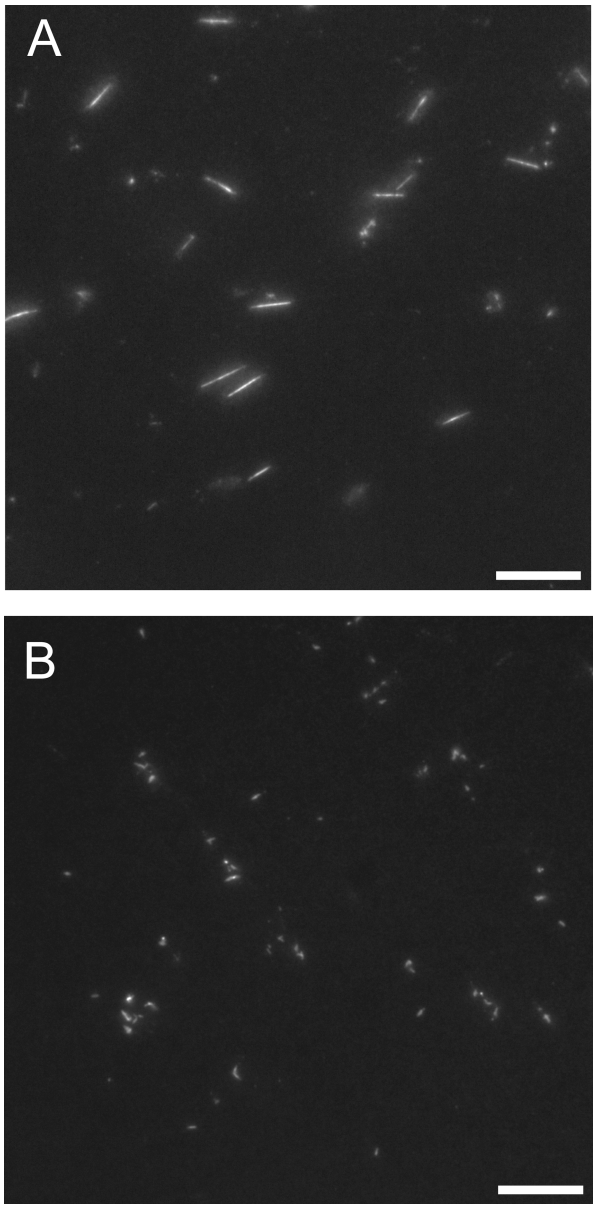

FIGURE 3: A22-mediated inhibition of MreB assembly visualized by fluorescence microscopy. MreB (1 μM, 20% Alexa488-labeled) was polymerized in 10 mM imidazole (pH 7.0), 1 mM $MgCl_2$, 1 mM EGTA, 20 mM KCl, and 200 μM ATP at 20 °C for 1 h in the absence (A) or presence (B) of 300 μM A22 and imaged directly by epifluorescence microscopy. The scale bar is 10 μm.

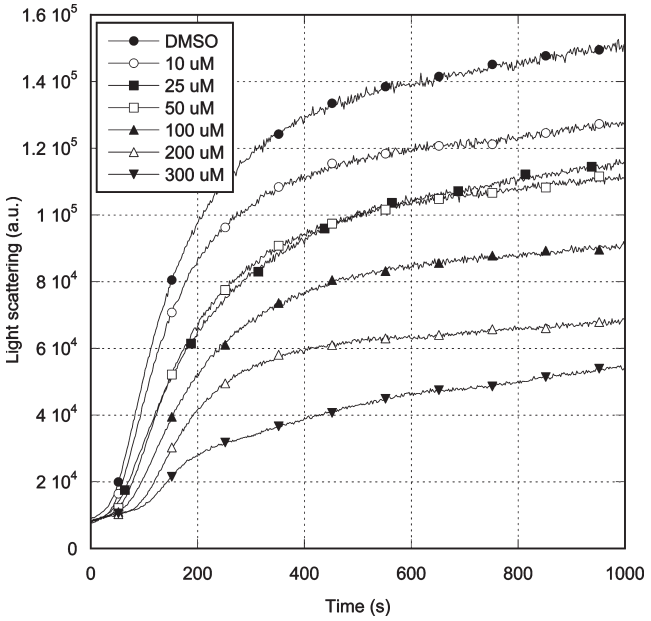

FIGURE 4: Effects of A22 on MreB polymerization time course. MreB (5 μM) was polymerized in 10 mM imidazole (pH 7.0), 20 mM KCl, 1 mM $MgCl_2$, and 200 μM ATP at 20 °C in the presence of varying concentrations of A22. The MreB polymerization time course was followed by 400 nm right angle light scattering. A22 concentrations are as specified in the inset.

secondary binding of A22 to MreB caused protein aggregation and massive, rapid increases in light scattering intensity (not shown). Similar experiments using ADP-bound MreB produced no observable effect over the same concentration range (Figure 1 of the Supporting Information).

A22 Increases the Critical Concentration for MreB Assembly. We previously measured the critical concentration for assembly of MreB under varying nucleotide, temperature, and buffer conditions (*29*). Here we have investigated the effects of A22 on the critical concentration of MreB. We allowed MreB to assemble to steady state at varying concentrations under standard reaction conditions in the presence of ATP and measured the light scattering intensity. A plot of light scattering intensity versus protein concentration (Figure 5A) demonstrated a characteristic biphasic behavior, with two independent linear distributions of data points. The concentration at which the data inflect upward represents the critical concentration, equivalent to the affinity of monomers for polymers or the concentration above which polymerization occurs. In the absence of A22, in ATP at 20 °C, MreB exhibited a critical concentration of 500 nM. When A22 was included at its maximal inhibitory concentration of 300 μM, the critical concentration was shifted to approximately 2000 nM (Figure 5B).

A22 Shifts the Monomer−Polymer Equilibrium in the Sedimentation Assay. MreB polymers pellet when subjected to ultracentrifugation, but monomers remain in solution. We polymerized 5 μM MreB in standard buffer conditions in the presence of ATP at 4 or 20 °C in the presence or absence of 300 μM A22. At 4 °C, approximately 40% of MreB pelleted in the absence of A22, consistent with the previously determined critical concentration of 2000 nM under identical conditions (Figure 6). In the presence of A22, however, virtually all MreB remained in the supernatant at 4 °C, consistent with a temperature-dependent increase in the critical concentration. At 20 °C, approximately 90% of MreB pelleted in the absence of A22, consistent with the previously measured critical concentration of 500 nM. Addition of A22 decreased the fraction of MreB recovered in the pellet to approximately 60%, which is consistent with the presently determined critical concentration of approximately 2000 nM. In parallel experiments in the presence of ADP, A22 produced no observable change in the fraction of MreB pelleted (Figure 2 of the Supporting Information).

DISCUSSION

Gitai et al. (*16*) isolated seven A22-resistant missense mutants in *C. crescentus* and found that each mapped to the nucleotide-binding cleft of MreB. This observation made a strong implicit case for MreB as the target of A22 but did not rule out alternative targets and provided no explanation for the mechanism of A22's possible effect on MreB.

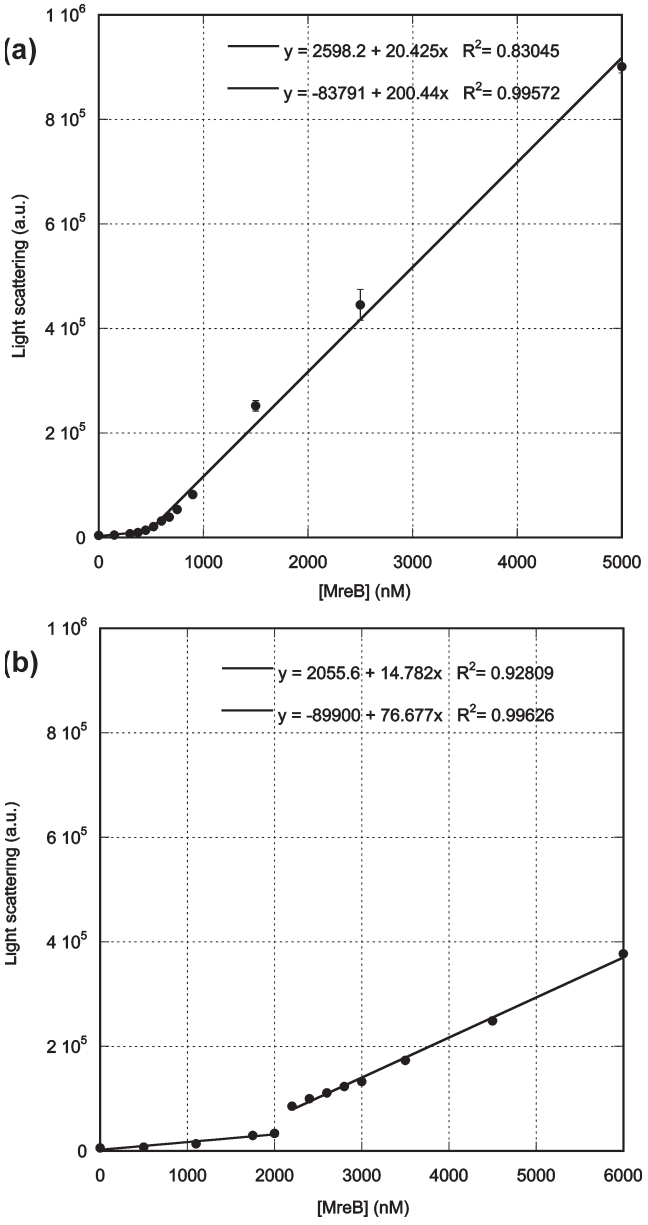

FIGURE 5: Effect of A22 on the MreB critical concentration. Varying concentrations of MreB were polymerized at 4 °C overnight in 10 mM imidazole (pH 7.0), 1 mM $MgCl_2$, 1 mM EGTA, 20 mM KCl, and 200 μM ATP in the absence (A) or presence (B) of 300 μM A22. Samples were equilibrated to 20 °C for 1 h, and the 400 nm light scattering intensity was measured. Linear fits to the data yielded critical concentrations of 500 (A) and 2000 nM (B).

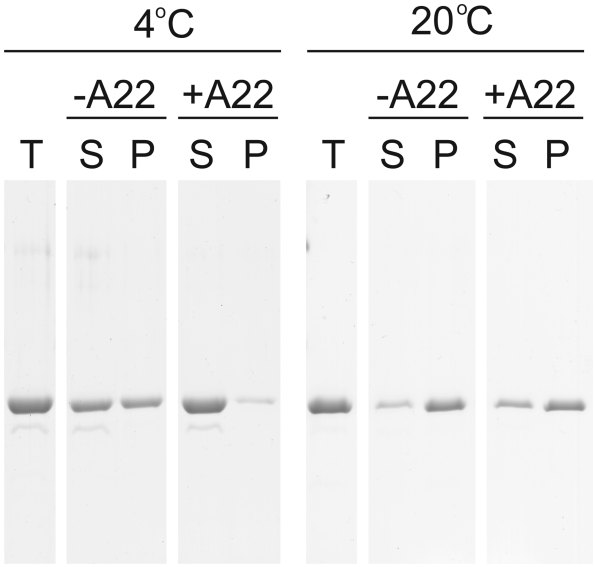

FIGURE 6: Effects of A22 on sedimentation of MreB. MreB (5 μM) was polymerized for 1 h at 4 or 20 °C in 10 mM imidazole (pH 7.0), 1 mM $MgCl_2$, 1 mM EGTA, 20 mM KCl, and 200 μM ATP in the presence or absence of 100 μM A22. Samples were centrifuged at 4 or 20 °C for 30 min at 100000*g*. Equivalent volumes of total (T), supernatant (S), and pellet (P) samples are shown by SDS−PAGE and Coomassie Blue.

The NMR experiments described in this paper represent the first evidence for a direct interaction between A22 and MreB. We found that A22 binds nucleotide-free MreB with a K_d of not greater than 1.3 μM. This value is much lower than the concentrations of A22 typically used in cellular assays and the measured minimum inhibitory concentration for A22 and its derivatives (*22*). This observation is likely due to the competitive binding of A22 and ATP and the high cellular ATP concentration. MreB binds ATP with submicromolar affinity (unpublished observations). Therefore, in cytoplasm or experiments that include millimolar levels of ATP, A22 must be used at concentrations much greater than its K_d to saturate binding.

Our docking studies suggest that A22 binds with high affinity and specificity in the nucleotide-binding pocket of MreB, overlapping with the position that would otherwise be occupied by the β- and γ-phosphates of ATP. The two MreB residues that interact most directly with A22 are E131 and T158. Both residues are conserved among all MreBs, but not in eukaryotic actins or the plasmid-encoded actin ParM. Significantly, the A22 resistance mutation most frequently found in *C. crescentus* by Gitai et al. was T176A, which corresponds to T158 in *T. maritima*. Thus, the mechanism of resistance in that mutation is likely to be a simple failure of the mutant MreB to bind A22. Viewed in concert, these results explain the failure of A22 to affect eukaryotic actins and ParM.

We observed the direct disruption of MreB assembly by A22 in a variety of biochemical and microscopic assays. By epifluorescence microscopy, we found that A22 inhibits the normal assembly of MreB into large, rigid polymers, producing instead only small, poorly defined clumps of fluorescence. We also observed A22 to inhibit the time course of MreB assembly in a bulk light scattering assay, with maximal inhibition at 300 μM A22. Competition with tightly bound ATP accounts for the high maximal inhibition concentration, similar to that observed in cells. At higher concentrations, A22 caused precipitation of MreB. The low-affinity, nonspecific association of A22 with the MreB surface identified in the docking studies may explain both this precipitation and the amorphous clumps observed by fluorescence microscopy.

Our measurement of the critical concentration for MreB polymerization in the absence and presence of A22 revealed that A22 binding causes a reduced affinity between MreB monomers and polymers. The critical concentration under polymerizing conditions at 20 °C shifted from 500 nM when bound to ATP to approximately 2000 nM when bound to A22. This value is similar to the value of 1700 nM measured for ADP-bound MreB (*29*). In all assays tested, A22 had no significant effects on MreB in the presence of ADP. We therefore hypothesize that A22-bound MreB is functionally if not structurally equivalent to the ADP-bound form. Experimental validation of this hypothesis will require atomic structures of both A22- and ADP-bound MreB.

The significance of the critical concentration increase is illustrated by our polymerization time course, sedimentation, and microscopy results. The time course of polymerization of 5 μM MreB was significantly reduced by A22 but not completely inhibited because the effective, polymerizable monomer concentration was effectively reduced from 4.5 to ~3 μM. Similarly, in the sedimentation assay, the fraction of MreB polymerized was reduced by A22 by approximately 1.5 μM, the difference between the critical concentrations with and without the drug. These experiments are directly relevant to the physiological effects of A22. Unlike eukaryotic actins, which are present in cytoplasm at concentrations of several hundred micromolar, MreB is present only in the low micromolar range (*3*). Thus, subtle shifts in the critical concentration can cause complete disassembly of the bacterial actin cytoskeleton. This predicts that the effects of A22 could be overcome by significant increases in the cellular MreB concentration. This is in contrast to the effects of known actin toxins, which stabilize filaments by binding multiple protomers or by capping filaments or sequestering monomers from the polymerizable pool (*32*). Because the effects of A22 are physiologically and biochemically subtle, it is possible that derivatives of the molecule may be identified whose structural effects, not only affinities, make them more attractive candidates for development as clinical antibiotics.

ACKNOWLEDGMENT

We thank Ryan Marcheschi for expert technical assistance with saturation transfer NMR experiments and data processing and Joshua Mayer for many helpful discussions.

SUPPORTING INFORMATION AVAILABLE

A22 had no observable effect on the time course or sedimentation behavior of MreB in the presence of ADP. This material is available free of charge via the Internet at http://pubs.acs.org.

REFERENCES

1. Bramhill, D., and Thompson, C. M. (1994) GTP-dependent polymerization of *Escherichia coli* FtsZ protein to form tubules. *Proc. Natl. Acad. Sci. U.S.A. 91*, 5813–5817.
2. Mukherjee, A., and Lutkenhaus, J. (1994) Guanine nucleotide-dependent assembly of FtsZ into filaments. *J. Bacteriol. 176*, 2754–2758.
3. Jones, L. J. F., Carballido-Lopez, R., and Errington, J. (2001) Control of Cell Shape in Bacteria: Helical, Actin-like Filaments in *Bacillus subtilis*. *Cell 104*, 913–922.
4. van den Ent, F., Amos, L. A., and Lowe, J. (2001) Prokaryotic origin of the actin cytoskeleton. *Nature 413*, 39–44.
5. Ausmees, N., Kuhn, J. R., and Jacobs-Wagner, C. (2003) The Bacterial Cytoskeleton: An Intermediate Filament-Like Function in Cell Shape. *Cell 115*, 705–713.
6. Pogliano, J. (2008) The bacterial cytoskeleton. *Curr. Opin. Cell Biol. 20*, 19–27.
7. Doi, M., Wachi, M., Ishino, F., Tomioka, S., Ito, M., Sakagami, Y., Suzuki, A., and Matsuhashi, M. (1988) Determinations of the DNA sequence of the mreB gene and of the gene products of the mre region that function in formation of the rod shape of *Escherichia coli* cells. *J. Bacteriol. 170*, 4619–4624.
8. Wachi, M., and Matsuhashi, M. (1989) Negative control of cell division by mreB, a gene that functions in determining the rod shape of *Escherichia coli* cells. *J. Bacteriol. 171*, 3123–3127.
9. Kruse, T., Moller-Jensen, J., Lobner-Olesen, A., and Gerdes, K. (2003) Dysfunctional MreB inhibits chromosome segregation in *Escherichia coli*. *EMBO J. 22*, 5283–5292.
10. Soufo, H. J. D., and Graumann, P. L. (2003) Actin-like Proteins MreB and Mbl from *Bacillus subtilis* Are Required for Bipolar Positioning of Replication Origins. *Curr. Biol. 13*, 1916–1920.
11. Kruse, T., and Gerdes, K. (2005) Bacterial DNA segregation by the actin-like MreB protein. *Trends Cell Biol. 15*, 343–345.
12. Figge, R. M., Divakaruni, A. V., and Gober, J. W. (2004) MreB, the cell shape-determining bacterial actin homologue, co-ordinates cell wall morphogenesis in *Caulobacter crescentus*. *Mol. Microbiol. 51*, 1321–1332.
13. Gitai, Z., Dye, N., and Shapiro, L. (2004) An actin-like gene can determine cell polarity in bacteria. *Proc. Natl. Acad. Sci. U.S.A. 101*, 8643–8648.
14. Defeu Soufo, H. J., and Graumann, P. (2005) *Bacillus subtilis* actin-like protein MreB influences the positioning of the replication machinery and requires membrane proteins MreC/D and other actin-like proteins for proper localization. *BMC Cell Biol. 6*, 10.
15. Iwai, N., Nagai, K., and Wachi, M. (2002) Novel S-benzylisothiourea compound that induces sperical cells in *Escherichia coli* probably by acting on a rod-shape-determining protein(s) other than penicillin-binding protein 2. *Biosci., Biotechnol., Biochem. 66*, 2658–2662.
16. Gitai, Z., Dye, N. A., Reisenauer, A., Wachi, M., and Shapiro, L. (2005) MreB Actin-Mediated Segregation of a Specific Region of a Bacterial Chromosome. *Cell 120*, 329–341.
17. Divakaruni, A. V., Ogorzalek Loo, R. R., Xie, Y., Loo, J. A., and Gober, J. W. (2005) The cell-shape protein MreC interacts with extracytoplasmic proteins including cell wall assembly complexes in *Caulobacter crescentus*. *Proc. Natl. Acad. Sci. U.S.A. 102*, 18602–18607.
18. Dye, N. A., Pincus, Z., Theriot, J. A., Shapiro, L., and Gitai, Z. (2005) Two independent spiral structures control cell shape in *Caulobacter*. *Proc. Natl. Acad. Sci. U.S.A. 102*, 18608–18613.
19. Nilsen, T., Yan, A. W., Gale, G., and Goldberg, M. B. (2005) Presence of multiple sites containing polar material in spherical *Escherichia coli* cells that lack MreB. *J. Bacteriol. 187*, 6187–6196.
20. Kruse, T., Blagoev, B., Lobner-Olesen, A., Wachi, M., Sasaki, K., Iwai, N., Mann, M., and Gerdes, K. (2006) Actin homolog MreB and RNA polymerase interact and are both required for chromosome segregation in *Escherichia coli*. *Genes Dev. 20*, 113–124.
21. Divakaruni, A., Baida, C., White, C., and Gober, J. W. (2007) The cell shape proteins MreB and MreC control cell morphogenesis by positioning cell wall synthetic complexes. *Mol. Microbiol. 66*, 174–188.
22. Iwai, N., Fujii, T., Nagura, H., Wachi, M., and Kitazume, T. (2007) Structure-activity relationship study of the bacterial actin-like protein MreB inhibitors: Effects of stubstitution of benzyl group in S-benzylisothiourea. *Biosci., Biotechnol., Biochem. 71*, 246–248.
23. Karczmarek, A., Martínez-Arteaga, R., Alexeeva, S., Hansen, F. G., Vicente, M., Nanninga, N., and den Blaauwen, T. (2007) DNA and origin region segregation are not affected by the transition from rod to sphere after inhibition of *Escherichia coli* MreB by A22. *Mol. Microbiol. 65*, 51–63.
24. Li, Z., Trimble, M. T., Brun, Y. V., and Jensen, G. J. (2007) The structure of FtsZ filaments in vivo suggests a force-generating role in cell division. *EMBO J. 26*, 4694–4708.
25. Robertson, G. T., Doyle, T. B., Du, Q., Duncan, L., Mdluli, K. E., and Lynch, A. S. (2007) A novel indole compound that inhibits *Pseudomonas aeruginosa* growth by targeting MreB is a substrate for MexAB-OprM. *J. Bacteriol. 189*, 6870–6881.
26. Srivastava, P., Demarre, G., Karpova, T. S., McNally, J., and Chattoraj, D. K. (2007) Changes in Nucleoid Morphology and Origin Localization upon Inhibition or Alteration of the Actin Homolog, MreB, of *Vibrio cholerae*. *J. Bacteriol. 189*, 7450–7463.
27. Noguchi, N., Yanagimoto, K., Nakaminami, H., Wakabayashi, M., Iwai, N., Wachi, M., and Sasatsu, M. (2008) Anti-infectious effects of S-benzylisothiourea compound A22, which inhibits the actin-like protein, MreB, in *Shigella flexneri*. *Biol. Pharm. Bull. 31*, 1327.
28. Uehara, T., and Park, J. T. (2008) Growth of *Escherichia coli*: Significance of Peptidoglycan Degradation during Elongation and Septation. *J. Bacteriol. 190*, 3914–3922.
29. Bean, G. J., and Amann, K. J. (2008) Polymerization Properties of the *Thermotoga maritima* Actin MreB: Roles of Temperature, Nucleotides, and Ions. *Biochemistry 47*, 826–835.
30. Mayer, M., and Meyer, B. (1999) Characterization of ligand binding by saturation transfer difference NMR spectroscopy. *Angew. Chem., Int. Ed. 38*, 1784–1788.
31. Morris, G. M., Goodsell, D. S., Halliday, R. S., Huey, R., Hart, W., Belew, R. K., and Olson, A. J. (1999) Automated docking using a Lamarckian genetic algorithm and an empirical binding free energy function. *J. Comput. Chem. 19*, 1939–1662.
32. Morton, W. M., Ayscough, K. R., and McLaughlin, P. J. (2000) Latrunculin alters the actin-monomer subunit interface to prevent polymerization. *Nat. Cell Biol. 2*, 376–378.